String-Averaging Expectation-Maximization for Maximum Likelihood Estimation in Emission Tomography

Elias Salomão Helou[1], Yair Censor[2], Tai-Been Chen[3], I-Liang Chern[4,5], Álvaro Rodolfo De Pierro[6], Ming Jiang[7] and Henry Horng-Shing Lu[8]

[1]Department of Applied Mathematics and Statistics, State University of São Paulo, Postal Box 668, São Carlos, SP, Brazil. elias@icmc.usp.br.

[2]Department of Mathematics, University of Haifa, Mt. Carmel, Haifa 3190501, Israel. yair@math.haifa.ac.il.

[3]Department of Medical Imaging and Radiological Sciences, I-Shou University, Kaohsiung City, Taiwan 82445, ROC. ctb@isu.edu.tw.

[4]Department of Applied Mathematics, Center of Mathematical Modeling and Scientific Computing, National Chiao Tung University, Hsin Chu, Taiwan 30010, ROC. chern@math.ntu.edu.tw.

[5]Department of Mathematics, National Taiwan University, Taipei, Taiwan 10617, ROC. chern@math.ntu.edu.tw.

[6]Department of Applied Mathematics and Statistics, State University of São Paulo, Postal Box 668, São Carlos, SP, Brazil. alvaro@ime.unicamp.br.

[7]LMAM, School of Mathematical Sciences, Beijing International Center for Mathematical Research, Peking University, Beijing 100871, China. ming-jiang@ieee.org.

[8]Institute of Statistics, National Chiao Tung University, 1001 University Road, Hsinchu, Taiwan 30010, ROC. hslu@stat.nctu.edu.tw.

arXiv:1402.2455v1 [physics.med-ph] 11 Feb 2014

May 4, 2013. Revised: December 2, 2013. Revised: January 30, 2014.

Abstract

We study the maximum likelihood model in emission tomography and propose a new family of algorithms for its solution, called String-Averaging Expectation-Maximization (SAEM). In the String-Averaging algorithmic regime, the index set of all underlying equations is split into subsets, called "strings," and the algorithm separately proceeds along each string, possibly in parallel. Then, the end-points of all strings are averaged to form the next iterate. SAEM algorithms with

several strings presents better practical merits than the classical Row-Action Maximum-Likelihood Algorithm (RAMLA). We present numerical experiments showing the effectiveness of the algorithmic scheme in realistic situations. Performance is evaluated from the computational cost and reconstruction quality viewpoints. A complete convergence theory is also provided.

Index Terms

Emission tomography (ET), String-averaging, Block-iterative, Expectation maximization (EM) algorithm, Ordered subsets expectation maximization (OSEM) algorithm, Relaxed EM, String-averaging EM algorithm.

I. Introduction

The Expectation-Maximization (EM) algorithm (see, e.g., [1, Chapter 7] or [2]) has become a household tool for Maximum Likelihood Estimation (MLE) in Emission Tomography (ET). The original EM algorithm is *simultaneous* since when passing from a current iterate x^k to the next one x^{k+1}, *all* equations $\langle a^i, x\rangle = b_i$, $i = 1, 2, \cdots, m$, in the linear system $Ax = b$ of the underlying problem are used. In contrast to this, there is the Row-Action Maximum Likelihood Algorithm (RAMLA) (of Browne and De Pierro [3]) which is structurally *sequential* since each iteration k involves *only one* equation $\left\langle a^{i(k)}, x\right\rangle = b_{i(k)}$, where $i(k)$ is one of the indices $\{1, 2, \ldots, m\}$ chosen at the k-th iteration, from the linear system of the underlying problem. In-between these two structural extremes we have also a block-RAMLA structure [3, Page 689] and the Ordered Subsets EM (OSEM) algorithm (of Hudson and Larkin [4]), both allowing to process in each iteration a "block" (i.e., a subset) of the m underlying equations, by applying to the equations of the block the simultaneous original EM iterative step. Section III brings a deeper discussion on alternative methods and related works.

In this article we propose and experiment with a new variant of the EM algorithm which uses *String-Averaging* (SA), thus we call the resulting algorithm the *SAEM algorithm*. In the SA algorithmic regime the index set of the m underlying equations is again split into subsets, now called "strings," and from a current iterate x^k the algorithm first proceeds sequentially along the indices of each string separately (which can be done in parallel) and then the endpoints of all strings are averaged to form the next iterate x^{k+1}. This is in stark contrast with how the above mentioned OSEM and block-RAMLA treat the equations of a block. Full details regarding the algorithm will be given on Section IV.

We advocate SAEM as a theoretically sound way to provide better quality in emission tomography image reconstruction. In order to support our claims, simulation studies performed with the intention to evaluate image quality and computational effort are reported on Section VI and a theoretical study of the convergence properties of the method can be found on Section V. Next section introduces the fundamentals of the problem and Section VII brings our concluding remarks.

II. ET image reconstruction: the problem, approaches and related works

Positron Emission Tomography (PET) and *Single Photon Emission Tomography* (SPECT) are ideal modalities for in vivo functional imaging. Thus, ET can be used to monitor the

effects of therapy inside the living body or in oncological studies. The image reconstruction problem in ET can be fully-discretized and modeled by a system of linear equations [13]:

$$Ax = b \tag{1}$$

where the measured data is $b = (b_i)_{i=1}^m \in \boldsymbol{R}^m$, the image vector is $x = (x_j)_{j=1}^n \in \boldsymbol{R}^n$, and A is an $m \times n$ real matrix, and the problem is to estimate the image vector x from the measured data b. Solution of this system by classical direct elimination methods will likely be impractical because of the huge data and image dimensions, ill-posedness of A coupled with noisy and/or incomplete data b, unstructured imaging matrix A, among several other well-known reasons [13], [14].

Instead, iterative methods, especially the row-action methods such as the algebraic reconstruction technique (ART) [20], [21], are usually applied for computationally efficient high-quality reconstruction [19]. Iterative algorithms have been important in this field because of their superior reconstructions over analytical methods in many instances, and their ability to handle the very large and sparse data associated with fully-discretized image reconstruction, see, e.g., [14], [15], [5], [16]. For reviews see, e.g., [17] and [18].

Another key advantage of iterative methods is their flexibility. For example, least-squares and *I*-divergence optimization approaches are commonly used for image reconstruction. In these approaches, the true image is estimated by the minimizer of an objective function, i.e., as a solution of a convex optimization problem. The least-squares functional is given by

$$L_{\text{LS}}(x) := \frac{1}{2}\|b - Ax\|^2, \quad \forall x \in \boldsymbol{R}^n. \tag{2}$$

ART is a prominent algorithm in this approach, which can be turned to be efficient for ET [19] even though it was originally proposed for x-ray tomography [20], [21]. The *I*-divergence (also called the Kullback-Leibler distance) functional is given by

$$L_{\text{KL}}(x) := I(b, Ax) = \sum_{i=1}^{m} b_i \log \frac{b_i}{\langle a^i, x\rangle} + \langle a^i, x\rangle - b_i, \quad \forall x \in \boldsymbol{R}^n_+, \tag{3}$$

where the vector $a^i = \left(a^i_j\right)_{j=1}^n$ is the transpose of the i-th row of A. From a statistical perspective, the least-squares approach is equivalent to finding an image as the maximum likelihood estimate from data with Gaussian noise, while the *I*-divergence approach does the same with Poissonian noise.

For the image reconstruction problem in ET, the *I*-divergence approach is more appropriate because Poissonian noise is dominant. The following iterative Maximum Likelihood

Expectation Maximization recursion, termed the MLEM (or the classical EM) algorithm, is popular since the 1980s [11] for the minimization of (3):

$$x_j^{k+1} := x_j^k \frac{1}{\sum_{i=1}^m a_j^i} \sum_{i=1}^m a_j^i \frac{b_i}{\langle a^i, x^k \rangle}, \quad \text{for } j = 1, 2, \cdots, n. \tag{4}$$

It was first proposed independently by Richardson [22] and Lucy [23] and for that reason is still known as the Richardson-Lucy (RL) algorithm in applications to astronomy and microscopy. It was later rediscovered in [9] and in [10] by applying the general expectation-maximization (EM) framework from statistics [24], [25] to the ET reconstruction problem.

In addition to the above two approaches, there are those which utilize other Bregman divergences (distances) and the Bayesian framework for image reconstruction [14], [13], of which the above least-squares and *I*-divergence approaches are special cases. In fact, SAEM can be readily generalized to cover these cases, because our analysis of convergence applies to the minimization of a general convex function over the nonnegative orthant.

From yet another perspective, the image reconstruction task can also be viewed as a *convex feasibility problem* (CFP) see [17]. Consequently the method based on projection onto convex sets (POCS) provides significant inspiration when developing iterative reconstruction algorithms, see, e.g., [14, Chapter 5] or [26]. There have been various iterative projection algorithms based on different kinds of projections such as the Euclidean, oblique and Bregman projections. Among them, the string-averaging projections (SAP) algorithmic scheme has attracted attention recently since its presentation in [27]. Therefore, the present paper brings an algorithmic bridge for this string-averaging scheme, going from the set theoretic to the maximum likelihood framework.

III. EM-TYPE ALGORITHMS

A. The classical EM algorithm

For A, a^i, b, and b_i, as defined above for $i \in I := \{1, 2, \cdots, m\}$, we define $R_{\text{EM}}^i : \boldsymbol{R}^n \to \boldsymbol{R}^n$ as the i-th row operator for the EM algorithm,

$$R_{\text{EM}}^i(x) := \frac{b_i}{\langle a^i, x \rangle} x. \tag{5}$$

For any index subset $B \subseteq I$, let $|B|$ denote the number of elements in B and let R_B be the averaging operator $R_B : \boldsymbol{R}^{|B| \times n} \to \boldsymbol{R}^n$ defined componentwise as

$$\left(R_B\left(\{y^i\}_{i \in B}\right)\right)_j := \frac{1}{\sum_{i=1}^m a_j^i} \sum_{i \in B} a_j^i y_j^i, \quad \text{for } j = 1, 2, \cdots, n. \tag{6}$$

The classical EM algorithm and many of its variants for image reconstruction are simultaneous algorithms, see, e.g., [14, Section 1.3] on the classification of iterative algorithms from the perspective of the algorithmic parallelization strategy. In pseudo-code, the classical EM algorithm, that uses (4), is as follows:

Algorithm III.1. *The Classical EM Algorithm*

$$
\begin{aligned}
&\textit{for } k = 0, 1, \cdots \\
&\quad \textit{for } i \in I \\
&\qquad x^{k+1,i} := R^i_{EM}(x^k), \qquad (7) \\
&\quad \textit{end} \\
&\quad x^{k+1} := R_I\left(\{x^{k+1,i}\}_{i\in I}\right). \qquad (8) \\
&\textit{end}
\end{aligned}
$$

It first executes simultaneously (in parallel) row-action operations on all rows from the same current iterate x^k. Then the intermediate iteration vectors $\{x^{k+1,i}\}_{i=1}^m$ are combined by the averaging operator R_I to obtain the next iterate.

B. The Block iterative EM algorithm

The classical EM algorithm can be accelerated by its block-iterative version [4], [28], [29]. A block-iterative version of a simultaneous algorithm, see [14, Section 1.3], employs the algorithmic operators R^i_{EM} and R_B as the simultaneous algorithm does, but it first breaks up the index set $I = \{1, 2, \cdots, m\}$ into "blocks" of indices so that for $t = 1, 2, \cdots, T$, the *block* B_t is a subset of I of the form

$$B_t := \left\{i^t_1, i^t_2, \cdots, i^t_{m(t)}\right\}. \qquad (9)$$

with $m(t)$ denoting the number of elements in B_t. The block-iterative version of the classical EM algorithm works as follows.

Algorithm III.2. *The Block-Iterative EM Algorithm*

$$
\begin{aligned}
&\textit{for } k = 0, 1, \cdots \\
&\qquad t = t(k) \in \{1, 2, \cdots, T\} \qquad (10)\\
&\qquad \textit{for } i \in B_t \\
&\qquad\qquad x^{k+1,i} := R^i_{EM}(x^k), \qquad (11)\\
&\qquad \textit{end} \\
&\qquad x^{k+1} := R_{B_t}\left(\{x^{k+1,i}\}_{i\in B_t}\right). \qquad (12)\\
&\textit{end}
\end{aligned}
$$

At the k-th iteration, the active block B_t is determined by the *control sequence* $t = t(k)$. Then, for each block the algorithm performs a simultaneous step as if the classical EM method was applied to this block alone and the iteration is updated. In the literature of maximum likelihood reconstruction for emission tomography, block-iterative EM algorithms are called "ordered-subsets EM" (OSEM) algorithms as they were named in the seminal work of Hudson and Larkin [4].

C. EM-type algorithms with relaxation

The OSEM algorithm has an improved experimental convergence rate, but may not converge when the system (1) is inconsistent [3]. This can be resolved by introducing relaxation as in the least-squares approach [39]. The first block-iterative EM algorithm with relaxation is the "row-action maximum likelihood algorithm" (RAMLA) in [3]. After statistical study of the noise propagation from the projection data to the reconstructed image, a modified version of the RAMLA, called "dynamic RAMLA" (DRAMA), using variable relaxation parameters with blocks, was proposed in [40]. A formula extending RAMLA and DRAMA was proposed in [41] as follows,

$$x^{k+1} = x^k - \lambda_{k,t} D(x^k) \nabla L^{B_t}_{\mathrm{KL}}(x^k), \qquad (13)$$

where $\lambda_{k,t}$ are stepsize parameters, $\nabla L^{B_t}_{\mathrm{KL}}$ is the gradient of the partial negative log-likelihood

$$L^{B_t}_{\mathrm{KL}}(x) := \sum_{i\in B_t} b_i \log \frac{b_i}{\langle a^i, x\rangle} + \langle a^i, x\rangle - b_i, \qquad (14)$$

and the pre-conditioner D is given by

$$D(x) := \operatorname{diag}\left\{\left(\frac{x_j}{p_j}\right) \mid 1 \le j \le n\right\}, \tag{15}$$

with positive constants $p_j > 0$. Possible choices of p_j are

$$p_j = \max_{1\le t\le T}\left\{\sum_{i\in B_t} a_j^i\right\}, \tag{16}$$

or

$$p_j = \frac{\sum_{i=1}^m a_j^i}{T}. \tag{17}$$

Convergence results established in [41] require that the following conditions are met:

Condition A: $x^0 \in \boldsymbol{R}_+^n$, $b \in \boldsymbol{R}_+^m$, $A \in \boldsymbol{R}_+^{m\times n}$, $\sum_{t=1}^T L_{\mathrm{KL}}^{B_t}(x) = L_{\mathrm{KL}}(x)$.

Condition B: rank $\left(W(x)^{\frac{1}{2}}A\right) = n$, where $W(x)^{\frac{1}{2}}$ is the component-wise square root of the diagonal matrix

$$W(x) = \operatorname{diag}\left\{\left(\frac{b_i}{\langle a^i, x\rangle^2}\right) \mid 1 \le j \le n\right\}. \tag{18}$$

This is equivalent to the strict convexity of the function $L_{\mathrm{KL}}(x)$.

Condition C: $0 < \lambda_{k,t} \le \lambda$, where λ is chosen such that

$$\lambda < \min\left\{\frac{p_j}{\sum_{i\in B_t} a_j^i} \mid 1 \le j \le n, 1 \le t \le T\right\}, \tag{19}$$

and, denoting $\lambda_k = \lambda_{k,1}$, such that

$$\sum_{k=0}^{\infty}\lambda_k = \infty; \quad \sum_{k=0}^{\infty}\lambda_k^2 < \infty; \quad \sum_{k=0}^{\infty}|\lambda_k - \lambda_{k,t}| < \infty; \tag{20}$$

$$\frac{\lambda_{k,t}}{\lambda_k} \to 1; \text{ and } \frac{\lambda_k}{\lambda_{k+1}} < \text{constant}. \tag{21}$$

The above assumptions on the relaxation parameters are very general and cover several situations of interest [40], [36], [47], [48]. If each block size is one, i.e., each block corresponds to one equation, then by using (13) and (15), we get the relaxed row-action iteration of RAMLA:

$$x_j^{k+1} = x_j^k + \lambda_{k,i}\frac{a_j^i}{p_j}\left(\frac{b_i}{\langle a^i, x^k\rangle} - 1\right)x_j^k, \text{ for } j = 1, 2, \cdots, n. \tag{22}$$

IV. THE STRING-AVERAGING SCHEME

A. The string-averaging prototypical scheme

The *string-averaging* (SA) algorithmic regime was originally formulated in [27] in general terms and applied there for solving the *convex feasibility problem* (CFP) with iterative projection algorithms, see, e.g., [27], [49], [50]. In the string-averaging paradigm, the index set $I = \{1, 2, \cdots, m\}$ is split into "strings" of indices. From the current iterate x^k, certain algorithmic operators (we shall call them *step operators* in the following) are applied sequentially along the indices of each string and the end-points of all strings are then combined by an additional algorithmic operator (which we name the *combination operator* from now on) to yield the next iteration vector.

To define SA algorithms precisely, the same decomposition as in (9) for the index set I is utilized. The *index set*

$$S_t := \left\{i_1^t, i_2^t, \cdots, i_{m(t)}^t\right\} = \left\{i_s^t |\ 1 \leq s \leq m(t)\right\} \tag{23}$$

is now serving as the *string* of indices in the current context, for $t = 1, 2, \cdots, T$. Viewed like that, strings and blocks are just names for index subsets $B_t \subseteq I$ or $S_t \subseteq I$ for $t = 1, 2, \cdots, T$. Interleaving of strings and blocks is possible, leading to algorithms with a tree-like parallelism structure, whose convergence properties can be almost directly devised from our analysis below.

Let us consider a set $Q \subset \boldsymbol{R}^n$ and family of operators $\{R^i\}_{i=1}^m$ mapping Q into itself, and an additional operator R which maps Q^T (i.e., the product of T copies of Q) into Q. In the SA paradigm these operators $\{R^i\}_{i=1}^m$ are the step operators and the operator R serves as the combination operator. The string-averaging prototypical scheme is as follows.

Algorithm IV.1. *The String-Averaging Prototypical Scheme [27]*

Initialization $x^0 \in Q$ *is an arbitrary starting point.*

Iterative Step *Given the current iterate* x^k,

(i) *for all* $t = 1, 2, \cdots, T$, *compute in parallel as follows: apply successively the step operator along the string* S_t,

$$x^{k+1,t} := R^{i_{m(t)}^t} \circ \cdots \circ R^{i_2^t} \circ R^{i_1^t}(x^k), \tag{24}$$

(ii) *apply the combination operator*

$$x^{k+1} := R\left(\{x^{k+1,i}\}_{t=1}^{T}\right). \tag{25}$$

For every $t = 1, 2, ..., T$, this algorithmic scheme first applies to x^k successively the step operators R^i whose indices i belong to the t-th string S_t. This can be done in parallel for all strings because the jobs of going along each string from (one and the same current iterate) x^k to the end-point $x^{k+1,t}$ are independent. Then the combination operator R maps all end-points onto the next iterate x^{k+1}. The iteration from x^k to x^{k+1} is called one cycle of iteration, whereas the iteration from x^k to $x^{k+1,t}$ is called the t-th sub-iteration in the k-th cycle. Notice that we can always obtain from this framework a *fully-sequential* algorithm by the choice $T = 1$ and $S_1 = I$ or a *fully-simultaneous* algorithm by the choice $T = m$ and $S_t = \{t\}$, $t = 1, 2, \cdots, T$.

B. The string-averaging EM algorithm

Here we merge the string-averaging algorithmic structure describe above with the maximum likelihood estimator in order to create the new string-averaging EM (SAEM) algorithm. To this end we adopt the row-action operation of RAMLA as step operators (22), namely:

$$(R^i_{\lambda_{k,i}}(x^k))_j := x^k_j + \lambda_{k,i}\frac{a^i_j}{p_j}\left(\frac{b_i}{\langle a^i, x^k\rangle} - 1\right)x^k_j, \text{ for } j = 1, 2, \cdots, n. \tag{26}$$

To combine end-points of strings we use convex combinations, thus, our algorithm takes the following form.

Algorithm IV.2. *The String-Averaging-EM (SAEM)*

Initialization *Choose parameters p_j, for $j = 1, 2, \cdots, n$, and parameters $\lambda_{k,i}$. Choose $x^0 > 0$ as an arbitrary initial vector, construct a family of strings $\{S_t\}_{t=1}^T$, choose a weight system $\{w_t\}_{t=1}^T$ such that $w_t > 0$ for all $t = 1, 2, \cdots, T$, and $\sum_{t=1}^T w_t = 1$.*

Iterative Step *Given the current iterate x^k,*

(i) *for all $t = 1, 2, \cdots, T$, compute (possibly in parallel) as follows: apply successively the RAMLA row-action iterative step given by (26) along the string S_t,*

$$x^{k+1,t} := R^{S_t}(x) := R^{i^t_{m(t)}} \circ \cdots \circ R^{i^t_2} \circ R^{i^t_1}(x^k), \tag{27}$$

where the dependence of each step operator in (27) on the relaxation parameter λ_{k,i_s^t}, $s = 1, 2, \cdots, m(t)$ has been left out for clarity.

(ii) *then combine the end-points by*

$$x^{k+1} = \sum_{t=1}^{T} w_t x^{k+1,t} \tag{28}$$

using the weights system $\{w_t\}_{t=1}^{T}$.

V. Theoretical Justification

In this section we provide a general justification for why SAEM algorithms present a convergent behavior. We base our proofs on the fact that the convex combination operator, used in the averaging step, preserves certain asymptotic characteristics of the step operator and, therefore, we can expect convergence whenever the step operator comes from a convergent algorithm as is the case here.

Incremental algorithms [43], such as those used for the stringing by the step operator of the SAEM algorithm satisfy an approximation given by

$$R^{S_t}(x, \lambda) = x - \lambda D(x) \nabla L^{S_t}(x) + O(\lambda^2), \tag{29}$$

according to Proposition V.3 below. In the current theory, the general form (29) allows us to prove convergence under suitable hypotheses for non-averaged algorithms, mainly because $L^{S_t} = L$ and, therefore, for such iterations we have:

$$x^{k+1} = x^k - \lambda_k D(x^k) \nabla L(x^k) + O(\lambda_k^2). \tag{30}$$

But any conclusion drawn from equation (30) should hold as well for a properly averaged algorithm, by replacing L by the following $\tilde{L}$:

$$\tilde{L}(x) := \sum_{t=1}^{T} w_t L^{S_t}(x), \tag{31}$$

where $w_t > 0$ are the weights. For the SAEM algorithm IV.2 with $\sum w_i = 1$, we have

$$x^{k+1} = x^k - \lambda_k D(x^k) \nabla \tilde{L}(x^k) + O(\lambda_k^2). \tag{32}$$

If the strings S_t are pairwise disjoint and such that $\bigcup_{t=1}^{T} S_t = \{1, 2, \ldots, m\}$ and $w_t = 1/T$, we have

$$x^{k+1} = x^k - \frac{\lambda_k}{T} D(x^k) \nabla L(x^k) + O(\lambda_k^2) \tag{33}$$

for the averaged iteration, and convergence will be towards the optimizer of $\tilde{L} = L$. In order to make the discussion more precise, from now on we consider the following general form of an averaging algorithm:

Algorithm V.1. *General Averaging Algorithm*

$$
\begin{aligned}
&\textit{for } k = 0, 1, \cdots \\
&\quad \textit{for } t = 1, 2, \ldots, T \\
&\qquad x^{k+1,t} := R^{S_t}(x^k, \lambda_k), \\
&\quad \textit{end} \\
&\quad x^{k+1} := \sum_{t=1}^{T} \omega_t x^{k+1,t} \\
&\textit{end}
\end{aligned}
$$

By considering this algorithm we cope with step operators R^{S_t} of a rather general form, but stick to the concrete realization of the combination operator. For this kind of iteration we have the following result.

Proposition V.2. *Suppose that* $\omega_t > 0$ *and* $\sum_{t=1}^{T} \omega_t = 1$ *in Algorithm V.1, and that for every* $t \in \{1, 2, \ldots, T\}$ *the following equality holds for all* $k \geq 0$*,*

$$
R^{S_t}(x^k, \lambda_k) = x^k - \lambda_k D(x^k) \nabla L^{S_t}(x^k) + O\big(\Gamma(\lambda_k)\big). \tag{34}
$$

Then we have

$$
x^{k+1} = x^k - \lambda_k D(x^k) \nabla \tilde{L}(x^k) + O\big(\Gamma(\lambda_k)\big), \tag{35}
$$

where $\tilde{L}$ *is defined in (31).*

Proof: The result is verified by observing that

$$
\begin{aligned}
x^{k+1} &= \sum_{t=1}^{T} \omega_t R^{S_t}(x^k, \lambda_k) \\
&= \sum_{t=1}^{T} \omega_t x^k - \lambda_k D(x^k) \nabla \sum_{t=1}^{T} \omega_t L^{S_t}(x^k) + \sum_{t=1}^{T} \omega_t O\big(\Gamma(\lambda_k)\big) \\
&= x^k - \lambda_k D(x^k) \nabla \tilde{L}(x^k) + O\big(\Gamma(\lambda_k)\big),
\end{aligned} \tag{36}
$$

where we have used the definition of the algorithm for the first equality, hypothesis (34) for the second, and then applied $\sum_{t=1}^{T}\omega_t = 1$, the definition of $\tilde{L}$, and a trivial property of the O notation to obtain the third equation. ■

We now prove the claim that our stringing operators R^{S_t} do satisfy an equation such as (34) with $\Gamma(\lambda_k) = \lambda_k^2$, as long as Lipschitz continuity holds for each parcel of $D(x^k)L^{S_t}(x^k)$ used during each stringing operation, according to the next statement.

Proposition V.3. *Let $L^{S_t} = \sum_{i\in S_t} L^i$ and $R^{S_t}(x,\lambda) := R_\lambda^{i_{m(t)}^t} \circ \cdots \circ R_\lambda^{i_2^t} \circ R_\lambda^{i_1^t}(x)$, where each R_λ^i for $i \in \{1,2,\cdots,m\}$ is given by*

$$R_\lambda^i(x) := x - \lambda D(x)\nabla L^i(x) \tag{37}$$

For $k = 1,2,\cdots$, denote

$$y^{k,0} := x^k, \tag{38}$$

$$y^{k,s} := R_{\lambda_k}^{i_s^t}(y^{k,s-1}), \quad s = 1,2,\cdots,m(t), \tag{39}$$

$$x^{k+1,t} := y^{k,m(t)} \tag{40}$$

$$x^{k+1} := \sum_{t=1}^{T} \omega_t x^{k+1,t}. \tag{41}$$

Assume that each $D(\cdot)\nabla L^{i_j^t}(\cdot)$ is Lipschitz continuous with a Lipschitz constant M and bounded by an upper bound N on the set $\{x^k, y^{k,s}\}_{k\in\mathbb{N},s\in I}$, then the operator R^{S_t} satisfies

$$R^{S_t}(x^k,\lambda_k) = x^k - \lambda_k D(x^k)\nabla L^{S_t}(x^k) + O(\lambda_k^2). \tag{42}$$

Proof: Unfolding of the definition of the operator leads to

$$R^{S_t}(x^k,\lambda_k) = x^k - \lambda_k \sum_{s=1}^{m(t)} D(y^{k,s-1})\nabla L^{i_s^t}(y^{k,s-1}). \tag{43}$$

Consider the magnitude of the following difference,

$$\epsilon^k := D(x^k)\nabla L^{S_t}(x^k) - \lambda_k \sum_{s=1}^{m(t)} D(y^{k,s-1})\nabla L^{i_s^t}(y^{k,s-1}), \tag{44}$$

which we can estimate as follows,

$$\left\|\epsilon^k\right\| = \left\| \sum_{s=1}^{m(t)} \left(D(x^k)\nabla L^{i_s^t}(x^k) - D(y^{k,j-1})\nabla L^{i_s^t}(y^{k,j-1}) \right) \right\| \tag{45}$$

$$\leq \sum_{s=1}^{m(t)} \left\| D(x^k)\nabla L^{i_s^t}(x^k) - D(y^{k,j-1})\nabla L^{i_s^t}(y^{k,j-1}) \right\| \tag{46}$$

$$\leq \sum_{s=1}^{m(t)} M \left\| x^k - y^{k,s-1} \right\|, \tag{47}$$

where the first inequality follows from the triangular inequality, and the latter from Lipschitz continuity. Now we notice that if $s > 1$, then

$$\|x^k - y^{k,s}\| = \left\| \lambda_k \sum_{l=1}^{s} D(y^{k,l-1})\nabla L^{i_l^j}(y^{k,l-1}) \right\| \leq \lambda_k mN \tag{48}$$

because of the boundedness hypothesis. Putting (47) and (48) together leads to $\|\epsilon^k\| \leq \lambda_k K$ for some large enough constant K, i.e., $\epsilon^k = O(\lambda_k)$. On the other hand, from (43) and (44)

$$R^{S_t}(x^k, \lambda_k) = x^k - \lambda_k D(x^k)\nabla L^{S_t}(x^k) + \lambda_k \epsilon^k, \tag{49}$$

which implies the assertion, since $\lambda O(\lambda) = O(\lambda^2)$. ■

We conclude by making the following connection.

Corollary V.4. *Under the assumptions of Propositions V.3 and V.2, Algorithm V.1 satisfies, for all* $k \geq 0$*,*

$$x^{k+1} = x^k - \lambda_k D(x^k)\nabla \tilde{L}(x^k) + O(\lambda_k^2). \tag{50}$$

Proof: Use Proposition V.3 followed by Proposition V.2. ■

So far we have shown how the string averaged iteration approximates a scaled gradient iteration. From now on we study how to obtain convergence from these approximate steps, which requires conditions on the sequence of parameters $\{\lambda_k\} \subset \boldsymbol{R}_+$. We will need $\sum_{k=1}^{\infty} \lambda_k = \infty$ because we will usually assume some sort of boundedness on $D(x^k)\nabla L(x^k)$ and, consequently, we would never reach optimal points if they happen to be too far away from the initial guess. On the other hand, if we do not impose $\lambda_k \to 0$, the error $O(\lambda_k^2)$ in the approximation does not necessarily vanish and will eventually dominate the computations when $\|D(x^k)\nabla L(x^k)\|$ becomes small. This must happen if we wish to converge to an optimal point since a necessary condition on a solution x^* for the non-negatively constrained problem

is $D(x^*)\nabla L(x^*) = 0$. We now show that, with no further hypotheses, at least one subsequence generated by the algorithm is of interest.

We will need the following lemma to prove the next proposition.

Lemma V.5. *(Lemma 2, [51]) Assume that $\{e_k\}$, $\{\nu_k\}$ and $\{d_k\}$ are sequences of non-negative numbers satisfying for all $k \geq 0$,*

$$e_{k+1} \leq e_k - \nu_k d_k \tag{51}$$

and that $\sum_{k=0}^{\infty} \nu_k = +\infty$. Then 0 is a cluster point of $\{d_k\}$.

Proposition V.6. *Suppose that the algorithm generating $\{x^k\}_{k\in\mathbb{N}}$ satisfies (50), $\sum_{k\in\mathbb{N}} \lambda_k = \infty$, $\lambda_k \to 0^+$, $\tilde{L}$ is smoothly differentiable and $\tilde{L}(x^k)$ is well-defined. Assume also that $\{x^k\} \subset \boldsymbol{R}^n_+$ is bounded. Then either $\lim \tilde{L}(x^k) = -\infty$ (i.e., the sequence of objective values is unbounded from below) or there is a subsequence l_k such that*

$$\lim_{l_k\to\infty} D(x^{l_k})\nabla\tilde{L}(x^{l_k}) = 0. \tag{52}$$

Proof: We first estimate how much does the objective function improve at each iteration. By using (50) followed by a first-order Taylor expansion we get:

$$\begin{aligned}\tilde{L}(x^{k+1}) &= \tilde{L}\left(x^k - \lambda_k D(x^k)\nabla\tilde{L}(x^k) + O(\lambda_k^2)\right)\\ &= \tilde{L}(x^k) - \lambda_k \nabla\tilde{L}(x^k)^T D(x^k)\nabla\tilde{L}(x^k) + O(\lambda_k^2).\end{aligned} \tag{53}$$

Then we rewrite the above equality as the following inequality, holding for some $M > 0$, by definition of $O(\lambda^2)$:

$$\tilde{L}(x^{k+1}) \leq \tilde{L}(x^k) - \lambda_k(\nabla\tilde{L}(x^k)^T D(x^k)\nabla\tilde{L}(x^k) - M\lambda_k) \tag{54}$$

Now suppose that $\nabla\tilde{L}(x^k)^T D(x^k)\nabla\tilde{L}(x^k)$ is bounded from below by a positive β. Then, for k large enough, the factor between parentheses in the second term of (54) will be nonnegative, satisfying the nonnegativity hypotheses of Lemma V.5. Therefore, if the sequence of objective values is bounded from below, it follows from Lemma V.5 that there is a subsequence l_k such that

$$\lim_{k\to\infty} \left\{\nabla\tilde{L}(x^{l_k})^T D(x^{l_k})\nabla\tilde{L}(x^{l_k}) + O(\lambda_{l_k})\right\} = 0. \tag{55}$$

Because $\lambda_k \to 0^+$, we have

$$\lim_{k\to\infty} \nabla\tilde{L}(x^{l_k})^T D(x^{l_k})\nabla\tilde{L}(x^{l_k}) = 0. \tag{56}$$

Consequently, for each $j = 1, 2, \cdots, n$,

$$\lim_{l_k\to\infty} D_j(x^{l_k}) \left(\partial_j\tilde{L}(x^{l_k})\right)^2 = 0. \tag{57}$$

By the boundeness assumption, we can assume that, with the same subsequence $\{l_k\}$,

$$\lim_{l_k\to\infty} D(x^{l_k}) = d, \tag{58}$$

for some $d \in \boldsymbol{R}^{n\times n}$. Hence, we obtain, for each $j = 1, 2, \cdots, n$,

$$\lim_{l_k\to\infty} \left(D_j(x^{l_k})\right)^2 \left(\partial_j\tilde{L}(x^{l_k})\right)^2 = d_{jj} \cdot 0 = 0. \tag{59}$$

Therefore, for each $j = 1, 2, \cdots, n$,

$$\lim_{k\to\infty} D_j(x^{l_k})\partial_j\tilde{L}(x^{l_k}) = 0, \tag{60}$$

from which the conclusion follows. ■

In particular, if it is known beforehand that $\tilde{L}$ is bounded from below, then we have shown that the algorithm does provide, at least, a useful subsequence. This is likely to be the case, since in real optimization problems (like in tomographic reconstruction), one will not be able to obtain an unboundedly good solution. Using the above result with some further assumptions (which include strict convexity) we obtain the following global convergence result.

Corollary V.7. *Suppose that the assumptions of Propositions V.3 and V.2 hold, assume also that $\tilde{L}$ is smoothly differentiable and strictly convex and that $\tilde{L}(x^k)$ is well-defined and that $\{x^k\} \subset \boldsymbol{R}^n_+$ is bounded. If $\tilde{L}(x^k)$ converges, then the sequence generated by Algorithm V.1 converges to the solution of*

$$\min_{x\in\boldsymbol{R}^n_+} \quad \tilde{L}(x).$$

Proof: If $\{x^k\}$ is bounded then we may assume, without loss of generality, that the subsequence which we have proven to exist in Proposition V.6 is convergent, say $x^{l_k} \to x^*$. If $x^* \in \boldsymbol{R}^n_+$ and $\tilde{L}$ is convex, then $D(x^*)\tilde{L}(x^*) = 0$ is a necessary and sufficient condition for x^* to be an optimal solution of problem (61).

By continuity, because $\tilde{L}(x^{l_k})$ converges, it must converge to $\tilde{L}(x^*)$. Therefore, the objective value at every accumulation point of $\{x^k\}$ equals $\tilde{L}(x^*)$. However, since we assumed that $\tilde{L}$

is strictly convex, this reasoning implies that all accumulation points of the bounded sequence $\{x^k\}$ are the same, namely x^*. Thus, we have proven that $x^k \to x^*$. ■

We now remove some of the hypotheses used in the last corollary by referring to works available in the literature. This leads to our main result, stated below.

Theorem V.8. *Assume that all components of $x^0 \in \boldsymbol{R}^n_+$ are positive, $0 < \lambda_k \leq \lambda$ for some suitably small $\lambda > 0$, $\sum_{k=0}^{\infty} \lambda_k = \infty$ and $\sum_{k=0}^{\infty} \lambda_k^2 < \infty$. Then, if L is the negative Poisson log-likelihood and if $\tilde{L}$ is strictly convex, then the sequence generated by Algorithm V.1 converges to the solution of (61).*

Proof: Boundedness of $\{x^k\}$, for small enough λ_k, is a consequence of [3, Proposition 1]. Convergence of $\tilde{L}(x^k)$ may then be obtained by assuming that $D(x)\nabla\tilde{L}(x)$ is Lipschitz continuous on the closure of the convex hull of the iterates and that $\sum_{k=0}^{\infty} \lambda_k^2 < \infty$, as in [36, Lemma 3]. Furthermore, we see that, if $\lambda_k \leq \lambda$ for some suitably small $\lambda > 0$, it is possible to adapt the ideas leading to [41, Corollary 1] to our case, yielding the conclusion that $D(x)\tilde{L}(x)$ is Lipschitz continuous within the closure of the convex hull of the iterates (and subiterates) of the averaged algorithm (V.1). Therefore, since $\tilde{L}$ is naturally bounded from below, we can apply Corollary V.7. ■

VI. Experimental work

This section is devoted to the experimental setup we have used in order to test the practical usefulness of SAEM algorithms and the results obtained. We will base our conclusions in two different figures of merit, the first is the squared error from the ground truth image, and the second being a Total-Variation based analysis, which puts on firmer grounds our claims about image quality. In what follows we provide a detailed description of the experimental setup. Subsection VI-A will report the experimental results.

There are certain sources of pseudo-randomness in the numerical experiments we have performed, such as the choice of strings and the noise simulations, but the presented results are representative of the typical situation, as we have noticed little deviation from this behavior from one run to another of the experiments. Moreover, to enable any interested reader to reproduce our research, the full source code of the numerical algorithms used in this paper is available upon request.

a) Data Generation: In our simulated studies we used the modified Shepp-Logan head phantom [9] in order to compare the quality of images reconstructed by RAMLA and SAEM. Let us define the so-called Radon transform $\mathcal{R}[f]$ of a function $f : \mathbf{R}^2 \mapsto \mathbf{R}$:

$$\mathcal{R}[f](\theta, t) := \int_{\mathbf{R}} f\big(t(\cos\theta, \sin\theta)^T + s(-\sin\theta, \cos\theta)^T\big)\mathrm{d}s.$$

Figure 1 shows a schematic representation of the basic geometry of the Radon transform. The Shepp-Logan phantom is shown, together with its sinogram, i.e., its Radon transform presented as an image in the $\theta \times t$ coordinate system.

We have used a parallel beam geometry where the samples were measured at the pairs (θ, t) in the set $\{\theta_1, \theta_2, \ldots \theta_v\} \times \{t_1, t_2, \ldots, t_r\}$ where $\theta_i = \pi(i-1)/v$ and $t_j = -1+2(j-1)/(r-1)$ for $1 \leq i \leq v$ and $1 \leq j \leq r$. That is, we uniformly sample the Radon transform on the box $[0, \pi) \times [-1, 1]$. Data was generated as samples of a Poisson random variable having as parameter the exact Radon transform of the scaled phantom:

$$b_i \sim Poisson\big(\kappa\mathcal{R}[f](\theta_{v_i}, t_{r_i})\big), \quad 1 \leq i \leq vr, \tag{61}$$

where v_i is one plus the largest integer smaller than $(i-1)/r$, $r_i = i - r(v_i - 1)$, and where the scale factor $\kappa > 0$ is used to control the simulated photon count, i.e., the noise level. We will also denote the vector $b^\dagger$ as the one with ideal data: $b_i^\dagger = \kappa\mathcal{R}[f](\theta_{v_i}, t_{r_i})$. In these studies, we have used $v = 288$ and $r = 256$ in order to reconstruct images consisting of 256×256 pixels.

We also experiment using data from a human cardiac SPECT study. In this set of experiments, the data set had $v = 60$ and $r = 64$ and we reconstructed images with 64×64 pixels. No attenuation correction has been applied to the data.

b) String Selection and Weights: We denote by SAEM-T an SAEM algorithm with T strings, and the strings were built by randomly shuffling the data and then partitioning it in T contiguous chunks of uniform size, each of which would become a string. It was done like that for two reasons. First, it is often recognized that a random order performs as well, if not better, than most other of practical viability in sequential algorithms. Second, this avoids unfair comparisons that could arise from specific choices of subsets, which could possibly be more suitable to one EM variant than to others.

We wanted to keep the classical maximum likelihood model, so we used non-weighted averaging, that is $\omega_i = 1/T$. More sophisticated weight selection schemes are conceivable, but this subject is beyond the scope of the present paper.

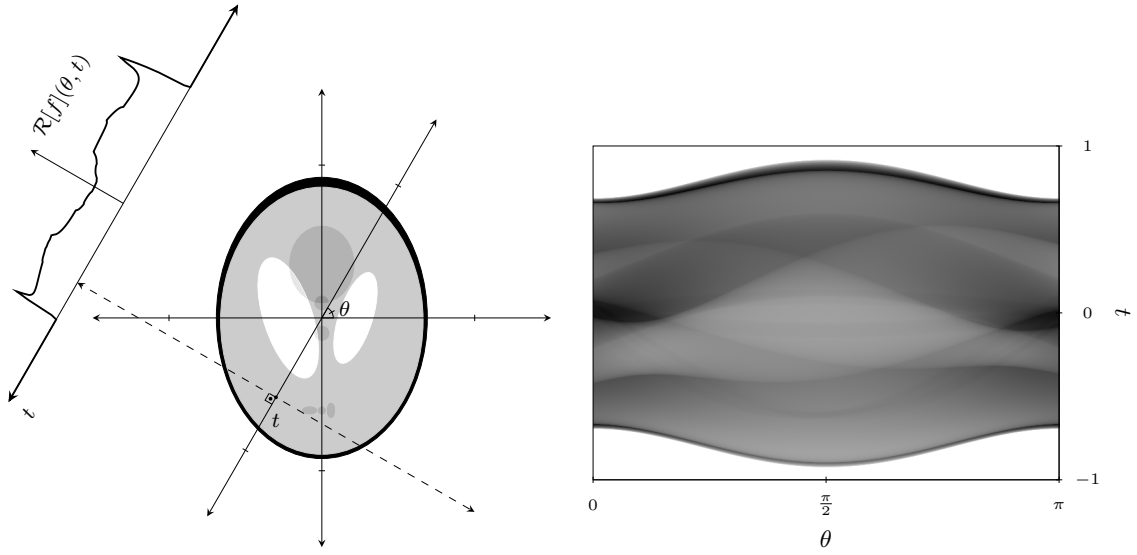

Fig. 1. Left: schematic representation of the Radon transform. In the definition, θ is the angle between the normal to the integration path and the vertical axis, while t is the displacement from origin of the line of integration. Right: Image of the Radon transform of the image shown on the left in the $\theta \times t$ coordinate system.

c) Scaling Matrix: In the algorithms we use, the scaling matrix $D(x)$ is a diagonal matrix with non-zero elements given by x_j/p_j for a fixed, but unspecified, set of weights $p_j > 0$. We have chosen $p_j = \sum_{i=1}^{n} a_{ij}$. Several other forms where possible, including some dependent on the particular method being used, but we chose to keep the experiments understandable and to have a uniform treatment among the algorithms, rather than to complicate the results introducing another varying parameter.

d) Stepsize: We are required to determine the nonsummable stepsize sequence $\{\lambda_k\} \subset \mathbf{R}_+$. We use the rule, for SAEM-T:

$$\lambda_k = \frac{\lambda_0^T}{k^{0.51}/T + 1}, \tag{62}$$

where λ_0^T was selected as the largest value for which SAEM-T would not lead to negative values in the first iteration. This technique for the starting parameter leads to the fastest possible convergence in terms of objective function decrease, and the scaling by the inverse of the number of strings accounts for the $1/T$ factor, caused by the averaging, in (33). Figure 2 shows that this is indeed a well balanced parameter rule, because it leads all SAEM variations to have similar log-likelihood values at any time point, as long as all the strings can be run simultaneously in hardware. It can also be seen that this behavior remains consistent under

several noise regimes. This same kind of plot is shown in the left-hand side of Figure 6 for the, smaller, real data example, where the comparison is no longer as balanced, because parallelism overhead does not pay off with small images, but in this case computation time is negligible anyway.

e) Starting Image: Initial guess for the algorithms was a uniform image with an expected photon count equal to the data. That is, $x_j^0 = \alpha$ where α is such that

$$\sum_{i=0}^{m}(Ax^0)_i = \sum_{i=0}^{m} b_i. \tag{63}$$

The value of α can be easily obtained as $\alpha = \sum_{i=0}^{m} b_i / \sum_{i=0}^{m}(A\mathbf{1})_i$, where $\mathbf{1}$ is the vector whose components are all equal to 1.

A. Image Reconstruction Analysis

Figure 2 shows that all SAEM-T algorithms present similar convergence speeds when measured as the ratio of objective function decrease and computation time. Notice that at iteration k, SAEM-T has a smaller log-likelihood value than SAEM-$(T+1)$. Hence, more strings means slower algorithms iteration-wise because there is less incrementalism present. It is widely recognized, however, that log-likelihood cannot be used as an image quality measure because over-fitting the image to the data will amplify high frequency components of the noise. This leads to the need for other ways of assessing reconstruction quality.

In the simulated studies, we make use of the mean squared error, which requires full knowledge about the ideal sought-after image:

$$MSE(x) := \frac{\|x - x^\dagger\|_2^2}{\|x^\dagger\|_2^2}, \tag{64}$$

where $x^\dagger$ is the noise-free discretization of the Shepp-Logan head phantom, properly scaled by κ. Another functional we have used to measure image quality was the Total Variation:

$$TV(x) := \sum_{i=1}^{r_1}\sum_{j=1}^{r_2}\sqrt{(x_{i,j} - x_{i,j-1})^2 + (x_{i,j} - x_{i-1,j})^2},$$

where $r_1 r_2 = n$ and we use the convention $x_{i,j} = x_{i(r_2-1)+j}$ for $i \in \{1, 2, \ldots, r_1\}$ and $j \in \{1, 2, \ldots, r_2\}$ with the boundary condition $x_{0,k} = x_{k,0} = 0$. Unlike the MSE, the Total Variation alone cannot be used as a measure of image quality. However, given two images of piecewise constant emission rates with the same Poisson likelihood, the one with the smaller Total Variation is more likely to have better image quality. Since neither the log-likelihood

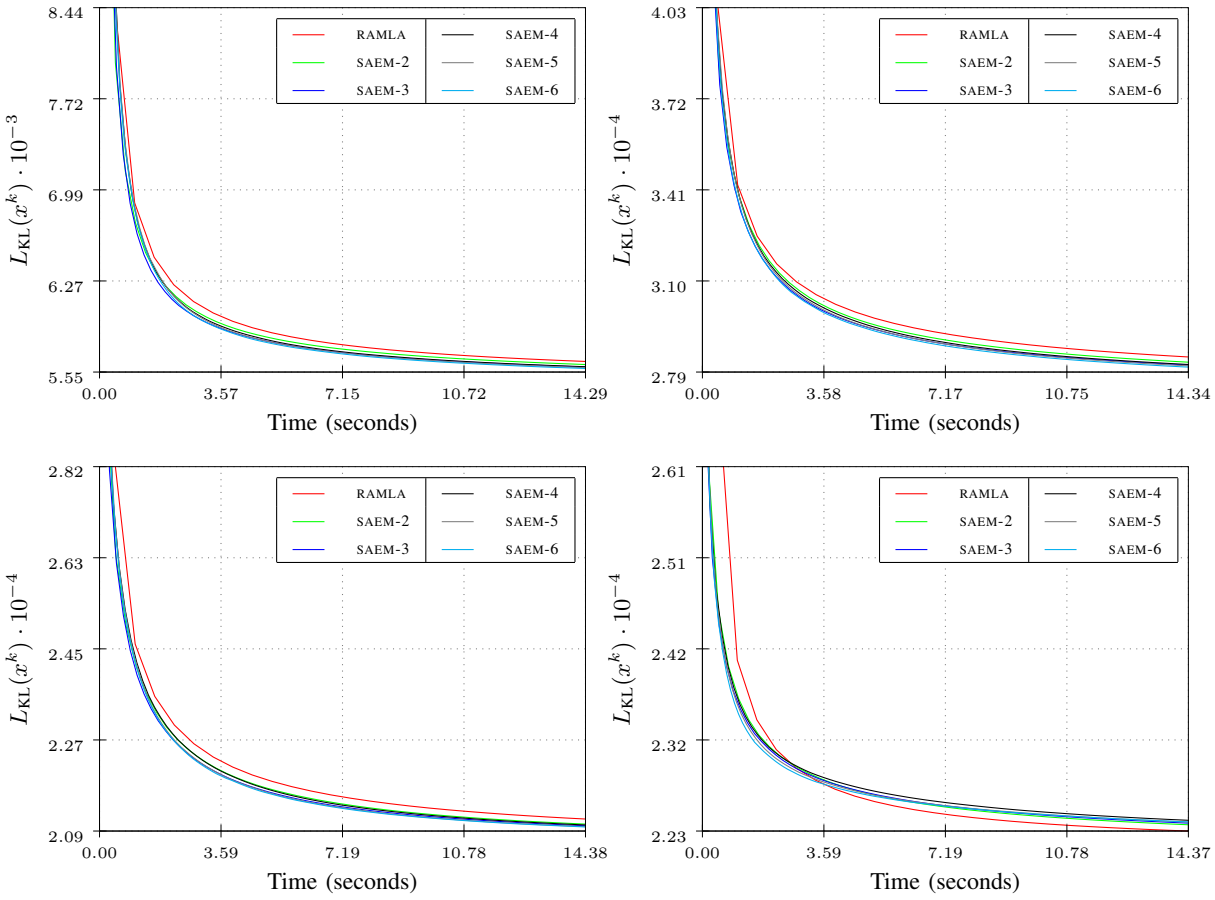

Fig. 2. Convergence speed of several SAEM variations under different noise condition. From top left in clockwise direction: 0.00%, 3.96%, 7.94% and 25.03% of relative noise $\|b - b^\dagger\|/\|b^\dagger\|$. Notice that if up to $T_{\max}$ strings can be run in parallel, then at any given time point, SAEM-T has similar log-likelihood values for $T = 1, \ldots, T_{\max}$. Running time was estimated by accumulating high-definition clock information of iteration computation, ignoring input/output time.

nor the Total Variation require knowledge of the ideal image, the combination of both can be used also in the evaluation of the SPECT reconstruction.

Figure 3 shows plots of both figures of merit as functions of the log-likelihood for one of the simulated experiments. On the left we have MSE and on the right TV. The remarkable feature of these plots is the fact that the quality of the image obtained by SAEM-T, at any given fixed likelihood level is an increasing function of T, the number of strings. This behavior is unaltered as we vary the noise level. Notice the same effect in the TV versus L_{KL} curve shown in the graphic at the right of Figure 6, and that the difference in the Total Variation translates into significant visual improvement in the real data study (Figure 7), even

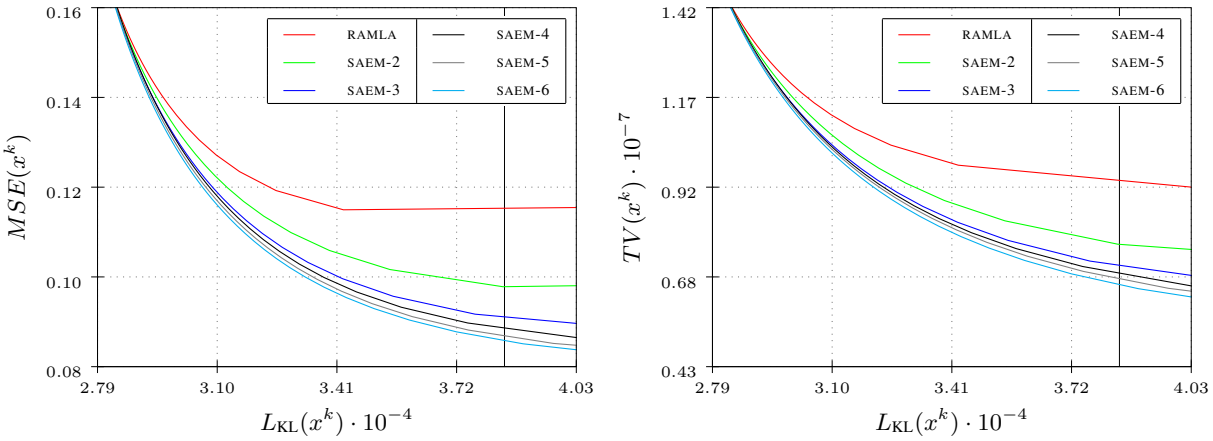

Fig. 3. Relative squared error and Total Variation as functions of the log-likelihood for iterations of SAEM variants. Notice that both the relative error and the Total Variation values, for a fixed likelihood level, are decreasing functions of the number of strings. The solid vertical lines show the log-likelihood level of the images of Figure 4.

more than it does in the simulated case (Figures 4 and 5).

VII. Conclusions

We have presented the new String-Averaging Expectation-Maximization family of algorithms. The theoretical convergence properties of the method were studied and experimental evidence was provided of the technique's suitability for good quality reconstruction in realistic settings.

The theory we have developed here can handle more general regularized objective functions, as they can achieve a better balance between smoothness and adherence to the data than traditional techniques currently used in tomographic scanners.

Future work could focus on comparative evaluation of SAEM against other paradigms, such as OS-EM or block-RAMLA, in light of the TV versus L_{KL} plots, which we have shown to be useful to assess image quality. It is potentially worth investigating *a posteriori* stopping criteria based on such plots, in the spirit of the L-curve [6].

Acknowledgments We are sincerely grateful to the anonymous reviewers whose insightful comments encouraged us to extend some of the experimental work in the paper. This resulted in discovering further advantages of the proposed SAEM algorithm in the final version.

Work by E. H. was partially supported by FAPESP grant 2013/16508-3, Brazil. Y. C. was partially supported by the United States-Israel Binational Science Foundation (BSF)

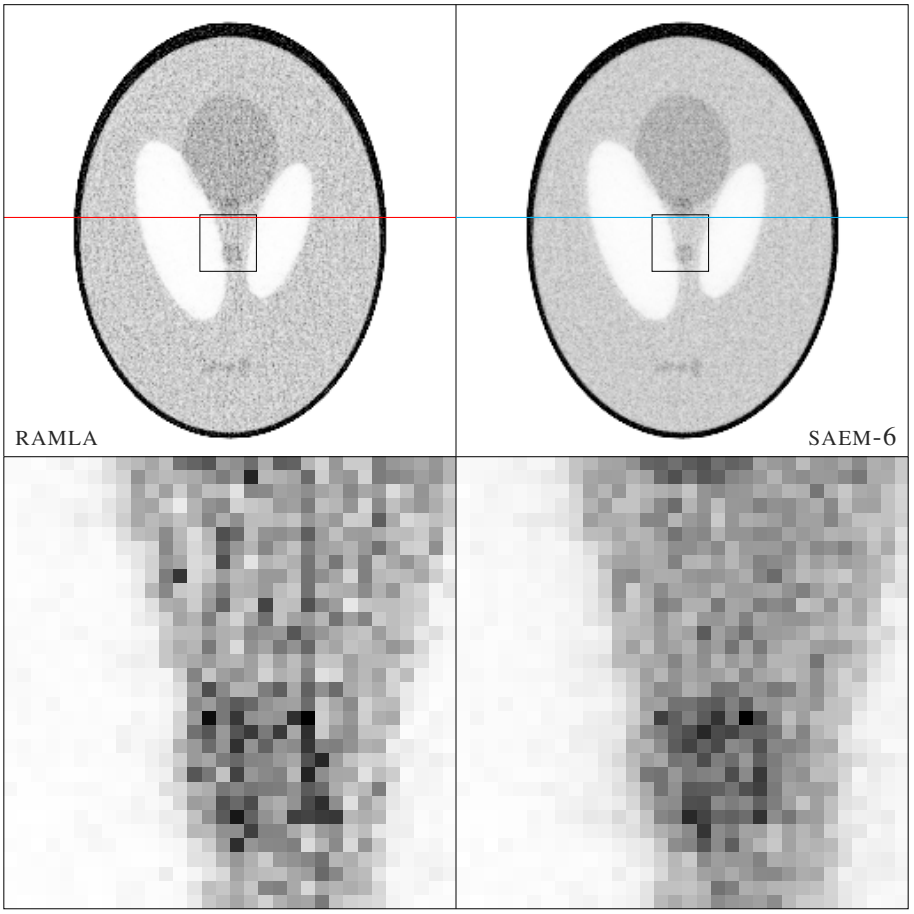

Fig. 4. Details of reconstruction obtained by RAMLA (left) and SAEM-6 (right). Both images where these details taken from have, up to linear interpolation errors, the log-likelihood level indicated by the solid vertical lines in Figure 3. It is noticeable that the smaller Total Variance is reflected in both smoother large areas and better resolved sharp transitions. The horizontal solid colored lines show where the profiles of Figure 5 where taken from.

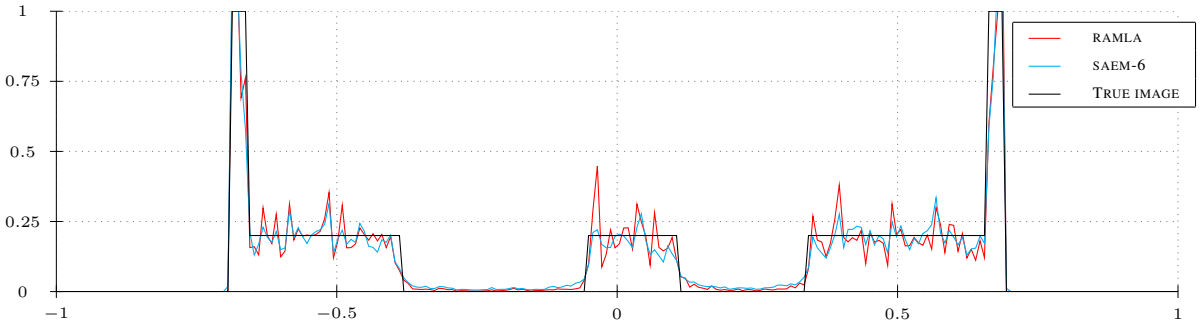

Fig. 5. Profile lines from images in Figure 4. Notice how SAEM-6 reconstruction presents less overshoot and more smoothness than RAMLA reconstruction.

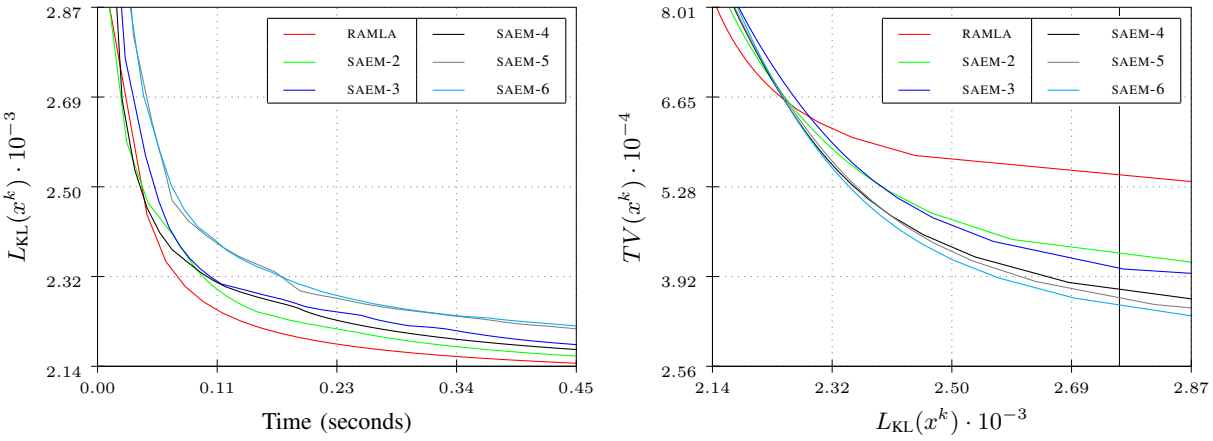

Fig. 6. Speed convergence and Total Variation results for the human SPECT study. The solid line in the graphic at the right indicates the log-likelihood level of the images in Figure 7.

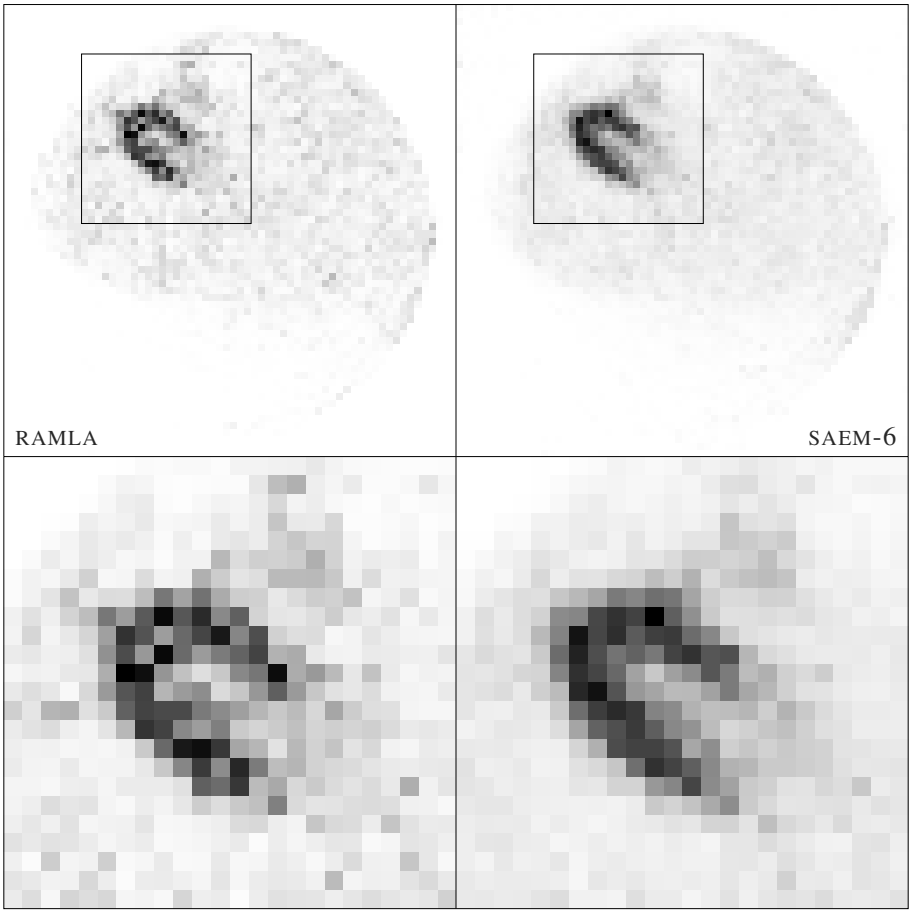

Fig. 7. Male human cardiac SPECT study. The log-likelihood level of the images is indicated by the solid lines in the graphic at the right in Figure 6. Data kindly provided by Roberto Isoardi – Fundación Escuela de Medicina Nuclear (FUESMEN) – Mendoza, Argentina

grant number 200912 and by US Department of Army award number W81XWH-10-1-0170. T. B. was partially supported by the National Science Council of the Republic of China, Taiwan (NSC 97-2118-M-214-001-MY2). I. C. was partially supported by the National Center for Theoretical Sciences (Taipei Office) and the National Science Council of the Republic of China (99-2115-M-002-003-MY3). A. D was partially supported by CNPq grant No 301064/2009-1, Brazil. M. J. was partially supported by the National Basic Research and Development Program of China (973 Program) (2011CB809105), National Science Foundation of China (61121002, 10990013, 60325101). H. L. was supported by grants from National Science Council, National Center for Theoretical Sciences, Center of Mathematical Modeling and Scientific Computing at National Chiao Tung University in Taiwan.

REFERENCES

[1] K. Lange, Optimization. New York: Springer, 2004.

[2] G. J. McLachlan and T. Krishnan, The EM algorithm and extensions, 2nd ed. Hoboken, N.J.: Wiley-Interscience, 2008.

[3] J. Browne and A. R. D. Pierro, "A row-action alternative to the EM algorithm for maximizing likelihood in emission tomography," IEEE Transactions on Medical Imaging, vol. 15, pp. 687 – 699, 1996.

[4] H. M. Hudson and R. S. Larkin, "Accelerated image reconstruction using ordered subsets of projection data," IEEE Transactions on Medical Imaging, vol. 13, pp. 601 – 609, 1994.

[5] R. Leahy and C. L. Byrne, "Recent developments in iterative image reconstruction for PET and SPECT," IEEE Transactions on Medical Imaging, vol. 19, pp. 257 – 260, 2001.

[6] P. C. Hansen, "Analysis of discrete ill-posed problems by means of the L-curve," Siam Review, vol. 34, 4, pp. 561 – 580, 1992.

[7] C. Johnson, J. Seidel, R. Carson, W. Gandler, A. Sofer, M. Green, and M. Daube-Witherspoon, "Evaluation of 3D reconstruction algorithms for a small animal PET camera," IEEE Transactions on Nuclear Science, vol. 44, pp. 1303 – 1308, 1997.

[8] A. Chatziioannou, J. Qi, A. Moore, A. Annala, K. Nguyen, R. Leahy, and S. Cherry, "Comparison of 3-D maximum a posteriori and filtered backprojection algorithms for high-resolution animal imaging with microPET," IEEE Transactions on Medical Imaging, vol. 19, pp. 507 – 512, 2000.

[9] L. A. Shepp and Y. Vardi, "Maximum likelihood restoration for emission tomography," IEEE Transactions on Medical Imaging, vol. 1, pp. 113 – 122, 1982.

[10] K. Lange and R. Carson, "EM reconstruction algorithms for emission and transmission tomography," Journal of Computer Assisted Tomography, vol. 8, pp. 306 – 316, 1984.

[11] Y. Vardi, L. A. Shepp, and L. Kaufman, "A statistical model for positron emission tomography," Journal of the American Statistical Association, vol. 80, pp. 8 – 20, 1985, with discussion.

[12] C. M. Chen, S. Y. Lee, and Z. H. Cho, "Parallelization of the EM algorithm for 3-D PET image reconstruction," IEEE Transactions on Medical Imaging, vol. 10, pp. 513 – 522, 1991.

[13] G. T. Herman, Fundamentals of Computerized Tomography: Image Reconstruction from Projections, 2nd ed. New York: Springer, 2009.

[14] Y. Censor and S. A. Zenios, Parallel Optimization: Theory, Algorithms and Applications. New York: Oxford University Press, 1997.

[15] J. A. Fessler, "Statistical image reconstruction methods for transmission tomography," in Handbook of Medical Imaging, M. Sonka and J. M. Fitzpatrick, Eds. Bellingham: SPIE, 2000, ch. 1, pp. 1 – 70.

[16] M. Jiang and G. Wang, "Development of iterative algorithms for image reconstruction," Journal of X-ray Science and Technology, vol. 10, pp. 77 – 86, 2002, invited Review.

[17] H. H. Bauschke and J. M. Borwein, "On projection algorithms for solving convex feasibility problems," SIAM Review, vol. 38, pp. 367 – 426, 1996.

[18] Y. Censor, W. Chen, P. L. Combettes, R. Davidi, and G. Herman, "On the effectiveness of projection methods for convex feasibility problems with linear inequality constraints," Computational Optimization and Applications, 2011, accepted for publication.

[19] G. T. Herman and L. B. Meyer, "Algebraic reconstruction techniques can be made computationlly efficient," IEEE Transactions on Medical Imaging, vol. 12, pp. 600 – 609, 1993.

[20] S. Kaczmarz, "Angenäherte auflösung von systemn linearer gleichungen," Bulletin International de l'Acadmie Polonaise des Sciences et Lettres, vol. 35, pp. 355 – 357, 1937.

[21] R. Gordon, R. Bender, and G. T. Herman, "Algebraic reconstruction techniques (ART) for three-dimensional electron microscopy and x-ray photography," Journal of Theoretical Biology, vol. 29, pp. 471 – 482, 1970.

[22] W. H. Richardson, "Bayesin-based iterative method od image restoration," Journal of the Optical Society of America, A, vol. 62, pp. 55 – 59, 1972.

[23] L. B. Lucy, "An iterative technique for the rectification of observed distribution," Astronomical Journal, vol. 79, pp. 745 – 754, 1974.

[24] A. P. Dempster, N. M. Laird, and D. B. Rubin, "Maximal likelihood form incomplete data via the EM algorithm," Journal of the Royal Statistical Society. Series B., vol. 39, pp. 1 – 38, 1977.

[25] M. Bertero, P. Boccacci, G. Desidera, and G. Vicidomini, "Image deblurring with poisson data: from cells to galaxies," Inverse Problems, vol. 25, pp. 123006, 2009.

[26] H. Stark and Y. Yang, Vector space projections : a numerical approach to signal and image processing, neural nets, and optics, ser. Wiley series in telecommunications and signal processing. New York: Wiley, 1998.

[27] Y. Censor, T. Elfving, and G. T. Herman, "Averaging strings of sequential iterations for convex feasibility problems," in Inherently parallel algorithms in feasibility and optimization and their applications (D. Butnariu, Y. Censor and S. Reich, Editors). Amsterdam: North-Holland, pp. 101 – 113, 2001.

[28] H. Zhu, J. Zhou, H. Shu, S. Li, and L. Luo, "Improved SAGE algorithm for PET image reconstruction using rescaled block-iterative method," in Engineering in Medicine and Biology Society, 2004. IEMBS'04. 26th Annual International Conference of the IEEE, vol. 1, pp. 1353 – 1356, 2004.

[29] C. Byrne, "Choosing parameters in block-iterative or ordered subset reconstruction algorithms," Image Processing, IEEE Transactions on, vol. 14, pp. 321 – 327, 2005.

[30] Y. Censor and T. Elfving, "Block-iterative algorithms with diagonally scaled oblique projections for the linear feasibility problem," SIAM Journal on Matrix Analysis and Applications, vol. 24, pp. 40 – 58, 2002.

[31] Y. Censor and G. T. Herman, "Block-iterative algorithms with underrelaxed bregman projections." SIAM Journal on Optimization, vol. 13, pp. 283 – 297, 2002.

[32] R. Davidi, G. T. Herman, and Y. Censor, "Perturbation-resilient block-iterative projection methods with application to image reconstruction from projections," International Transactions in Operational Research, vol. 16, pp. 505 – 524, 2009.

[33] F. Natterer, The Mathematics of Computerized Tomography. Philadelphia, PA: SIAM, 2001.

[34] C. L. Byrne, "Accelerating the EMML algorithm and related iterative algorithms by rescaled block-iterative methods," IEEE Transactions on Image Processing, vol. 7, pp. 100 – 109, 1998.

[35] A. R. De Pierro and M. E. B. Yamagishi, "Fast EM-like methods for maximum "a posteriori" estimates in emission tomography," IEEE Transactions on Medical Imaging, vol. 20, pp. 280 – 288, 2001.

[36] S. Ahn and J. A. Fessler, "Globally convergent image reconstruction for emission tomography using relaxed ordered subset s algorithms," IEEE Transactions on Medical Imaging, vol. 22, pp. 613 – 626, 2003.

[37] I. T. Hsiao, A. Rangarajan, P. Khurd, and G. Gindi, "An accelerated convergent ordered subsets algorithm for emission tomography," Physics in Medicine and Biology, vol. 49, pp. 2145 – 2156, 2004.

[38] Y. Censor, "Row-action methods for huge and sparse systems and their applications," SIAM Review, vol. 23, pp. 444 – 466, 1981.

[39] M. Jiang and G. Wang, "Convergence studies on iterative algorithms for image reconstruction," IEEE Transactions on Medical Imaging, vol. 22, pp. 569 – 579, 2003.

[40] E. Tanaka and H. Kudo, "Subset-dependent relaxation in block-iterative algorithms for image reconstruction in emission tomography," Physics in Medicine and Biology, vol. 48, pp. 1405 – 1422, 2003.

[41] E. S. Helou and A. R. De Pierro, "Convergence results for scaled gradient algorithms in positron emission tomography," Inverse Problems, vol. 21, pp. 1905 – 1914, 2005.

[42] R. Picard and D. Cook, "Cross-Validation of Regression Models," Journal of the American Statistical Association, vol. 79, pp. 575 – 583, 1984.

[43] E. S. Helou and A. R. De Pierro , "Incremental subgradients for constrained convex optimization: a unified framework and new methods", SIAM Journal on Optimization, 20, 3, 1547 – 1572, 2010.

[44] Engl, H.W., Hanke, M.. Nebauer, A, Regularization of Inverse Problems, Springer, 1996.

[45] M. Hanke and P.C. Hansen, "Regularization methods for large scale problems", Surveys Math. Indust., 3, 253 – 315, 1993.

[46] L.I. Rudin, S. Osher, E. Fatemi, "Nonlinear total variation based noise removal algorithms", Physica D, vol. 60, pp. 259 – 268, 1992.

[47] G. Wang and M. Jiang, "Ordered-subset simultaneous algebraic reconstruction techniques (OS-SART)," Journal of X-ray Science and Technology, vol. 12, pp. 169 – 177, 2004.

[48] E. Tanaka and H. Kudo, "Optimal relaxation parameters of DRAMA (dynamic RAMLA) aiming at one-pass image reconstruction for 3D-PET," Physics in Medicine and Biology, vol. 55, pp. 2917 – 2939, 2010.

[49] Y. Censor and E. Tom, "Convergence of string-averaging projection schemes for inconsistent convex feasibility problems," Optimization Methods & Software, vol. 18, pp. 543 – 554, 2003.

[50] S. N. Penfold, R. W. Schulte, Y. Censor, V. Bashkirov, S. McAllister, K. E. Schubert, and A. Rosenfeld, "Block-iterative and string-averaging projection algorithms in proton computed tomography image reconstruction," in Biomedical Mathematics: Promising Directions in Imaging, Therapy Planning and Inverse Problems, Y. Censor, M. Jiang, and G. Wang, Eds. Madison, WI: Medical Physics Publishing, 2010, pp. 347 – 367.

[51] M. R. Trummer, "Reconstructing pictures from projections: on the convergence of the ART algorithm with relaxation," Computing, vol. 26, pp. 189 – 195, 1981.